1988

Fine-structure mixing in 9 (2)D rubidium atoms by collisions with ground-state rubidium and noble gas atoms.

Tana Rei. Mallory
University of Windsor

NOTICE

The quality of this microform is heavily dependent upon the quality of the original thesis submitted for microfilming. Every effort has been made to ensure the highest quality of reproduction possible.

If pages are missing, contact the university which granted the degree.

Some pages may have indistinct print especially if the original pages were typed with a poor typewriter ribbon or if the university sent us an inferior photocopy.

Previously copyrighted materials (journal articles, published tests, etc.) are not filmed.

Reproduction in full or in part of this microform is governed by the Canadian Copyright Act, R.S.C. 1970, c. C-30.

AVIS

La qualité de cette microforme dépend grandement de la qualité de la thèse soumise au microfilmage. Nous avons tout fait pour assurer une qualité supérieure de reproduction.

S'il manque des pages, veuillez communiquer avec l'université qui a conféré le grade.

La qualité d'impression de certaines pages peut laisser à désirer, surtout si les pages originales ont été dactylographiées à l'aide d'un ruban usé ou si l'université nous a fait parvenir une photocopie de qualité inférieure.

Les documents qui font déjà l'objet d'un droit d'auteur (articles de revue, tests publiés, etc.) ne sont pas microfilmés.

La reproduction, même partielle, de cette microforme est soumise à la Loi canadienne sur le droit d'auteur, SRC 1970, c. C-30.

Canada

FINE-STRUCTURE MIXING IN 9 ^{2}D RUBIDIUM ATOMS BY COLLISIONS WITH GROUND-STATE RUBIDIUM AND NOBLE GAS ATOMS

by

Tana Rei Mallory

A Thesis
submitted to the
Faculty of Graduate Studies and Research
Through the Department of
Physics in Partial Fulfillment
of the Requirements for the Degree
of Master of Science at
the University of Windsor

Windsor, Ontario, Canada
1988

ISBN 0-315-43758-8

ABSTRACT

Using a method of two photon excitation, I have determined the cross sections for inelastic excitation transfer between 9 $^2D_{3/2}$ and 9 $^2D_{5/2}$ fine-structure states in rubidium induced in collisions with ground state rubidium atoms and noble gas atoms. Radiation from an N_2 laser-pumped dye laser, tuned to selectively excite one of the 9 ^2D sub-states, was made incident on rubidium vapour contained in a fluorescence cell. The resulting fluorescence consisted of two components: the direct component resulting from the originally excited state and the sensitized component resulting from the collisionally populated state. The cross sections for excitation transfer determined from the relative intensities of the fluorescence components were found to be:

Collision Partners.	Q_{34} $(9^2D_{3/2} \rightarrow 9^2D_{5/2})$ $(10^{-14} cm^2)$	Q_{43} $(9^2D_{3/2} \leftarrow 9^2D_{5/2})$ $(10^{-14} cm^2)$	$\frac{Q_{34}}{Q_{43}}$
Rb-He	9±3	6±2	1.45
Rb-Ne	6±2	3±1	1.91
Rb-Ar	26±9	17±6	1.50
Rb-Kr	42±15	23±8	1.79
Rb-Rb	91±32	62±22	1.48

Q_{34} and Q_{43} are the cross sections for transfer from the $9^2D_{3/2}$ to $9^2D_{5/2}$ fine-structure sub-state and from $9^2D_{5/2}$ to $92D_{3/2}$ sub-state respectively. The cross sections are considered to be accurate within ±35% and are in reasonable agreement with the ratio predicted by the principle of detailed balancing.

To Dad

ACKNOWLEDGEMENTS

I would like to thank Dr. L. Krause, under whose supervision this work was carried out, for his support and assistance during my time here.

I would also like to express my extreme gratitude for the patience and invaluable help offered to me by Dr. W. Kedzierski and by Dr. Randy Berends.

TABLE OF CONTENTS

LIST OF TABLES

LIST OF FIGURES

I INTRODUCTION

Since the discovery early in this century that when sodium, in a mixture with argon is irradiated with one of the D lines, the other D line will also show up in the fluorescence,[1] there have been many reports of experimental studies of transitions between fine-structure states in alkali-metals induced in collisions with various perturbers. Some of the first studies dealt with the ^2P resonance states and employed a resonance lamp for irradiation.[2,3,4] The intermediate and highly excited states remained inaccessible to detailed study until after the advent of tunable dye lasers.

Using tunable lasers it became possible to selectively populate a single fine-structure state. The excited atoms could then either decay radiatively to a lower state or be collisionally transferred to other fine-structure states, or decay non-radiatively to other lower lying levels. These processes are known as spontaneous decay, collisional excitation transfer and quenching (depopulation) of the excited state,

respectively.

The observed fluorescence emitted from an alkali metal vapour undergoing these changes consists of two components: the direct component, resulting from the decay of the optically excited state, and the sensitized component arising from the collisionally populated state. Since the sensitized component results from collisions with the neutral perturber, variation of the pressure, and thus the density of the perturber, produces a corresponding change in the ratio of sensitized-to-direct fluorescent intensities. From the variation of this ratio with perturber density it is possible to calculate the inelastic excitation transfer cross sections. Experiments of this type have been performed on rubidium n ^{2}p-5, n ^{2}S 6 and n ^{2}D [7,8,9] states, as well as various P, S, and D states in sodium,[10] cesium,[11] and potassium.[12] Several calculations have been reported, dealing with collisional fine-structure transitions and quenching of highly excited Rydberg atoms. De Prunelé and Pascale[13] carried out a calculation on the quenching of n^{2}D and n^{2}F alkali Rydberg states, and Omont[14] and Hahn[15] considered the collisions of Rydberg atoms with neutral perturbers. More recently Sirko and Rosinski[16] proposed a semi-classical model, similar to that of de Prunelé and

Pascale,[13] for fine-structure mixing in intermediate states of Rb and Cs atoms. Their calculations appear to be in good agreement with the experimental results for atoms excited to intermediate Rydberg states.

II THEORY

II.1 Collisional Processes

The size of a cross section for a given process is a measure of the probability of the process taking place. It can be considered as an area within which the particular event will occur with a 100% probability. In a classical sense this would be the area perpendicular to an incoming particle where a collision or scattering event would occur; no interaction would occur outside this area.

If we define b to be the radius of this area, or the impact parameter, then the scattering cross section $\sigma(v)$ is an integral over b, of some probability P(b,v):[13]

$$\sigma(v) = 2\pi \int_0^\infty db\, b\, P(b.v) \qquad (1)$$

where it is assumed that P(b,v)=1 for $0 < b < b_{max}$.

Since $\sigma(v)$ depends on the relative velocities of the two colliding partners, the more useful quantity is

$\langle\sigma(v)\rangle$, the cross section averaged over the relative velocity distribution of the two collision partners.

In an experimental situation such as a vapour or gas enclosed in a cell, the velocity distribution at a particular temperature is given by the Maxwell-Boltzman distribution:

$$\int_0^\infty dv\, v\, P(v,T) \tag{2}$$

Therefore, the measured cross section, Q(T), can be related to the cross section at a single velocity as follows:

$$Q(T) = 2\pi \frac{\int_0^\infty \left(\int_0^\infty db\, b\, P(b,v) \right) dv\, v\, P(v,T)}{\int_0^\infty dv\, v\, P(v,T)} \tag{3}$$

$$= \frac{\int_0^\infty dv\, v\, \sigma(v) P(v,T)}{\int_0^\infty dv\, v\, P(v,T)} \tag{4}$$

This investigation is concerned with the changes to the quantum state of excited rubidium atoms, (Rb*), induced by collisions with noble gases or ground state rubidium atoms. Since the Rb 9/ ^{2}D states are well separated from their nearest neighboring (n+2)S states,[17] these collisional changes can be considered to be mainly confined to the fine-structure doublet.[16] Thus the atom remains excited but is transferred to a different fine-structure quantum state. The change in kinetic energy is either absorbed or donated by the colliding partner. This process is called inelastic excitation transfer.

By analogy with gas-kinetic collisions, the frequency of collisions of an excited atom with a ground-state perturber, to produce excitation transfer, can be represented by:[18]

$$Z = N_g v Q(T) \qquad (5)$$

where N_g is the particle density of the ground-state atoms, v is the relative speed of the colliding partners, Q(T) is the cross section and Z is the frequency of

collision per excited atom.

If the perturber is electrically neutral-as is the case with noble gases- the interaction will be well localized, and the range will be shorter than the mean radius of the target atom.[13,15,16,19] In the case of atoms in intermediate or high Rydberg states the valence electron can be considered to be weakly bound to the ionic core and any collision between the perturber and the atom is essentially an interaction between the perturber and the valence electron, or the perturber and the ionic core. The interaction between the perturber and the ionic core is frequently neglected.

Assuming a model of interaction between the valence electron and the perturber, it is possible to obtain a measure of the relative size of the cross section by comparing it with the elastic electron-perturber cross section. The elastic scattering cross section, while one to two orders of magnitude smaller than the mixing cross sections, gives a measure of the relative strength of the interaction between the electron and the perturber.[8]

It is also possible, assuming no long range interactions, to compare the measured cross sections with the geometrical cross section of the excited atom. The

geometrical cross section is the area surrounding a Rydberg atom where the wave functions of the electrons have significant non-zero values and is given by:[20]

$$\sigma_g = \frac{1}{2}\pi a_0^2 n^{*2}\left[5n^{*2} + 1 - 3L(L-1)\right] \qquad (6)$$

where $n^*=7.66$ is the effective quantum number and $L=2$ is the angular momentum quantum number for the 9 ^2D, state and a_o is the Bohr radius. The contribution from the ground state atom is negligible compared to that of the excited atom.

Figure 1: A partial energy-level diagram (not to scale) of the Rb states involved in the excitation of the 9 ^2D states. Part a) represents the optical excitation of the 9 $^2D_{3/2}$ state and b) represents the optical excitation of the 9 $^2D_{5/2}$ state. The observed fluorescence components are labeled A, B, C, and D.

Figure 1

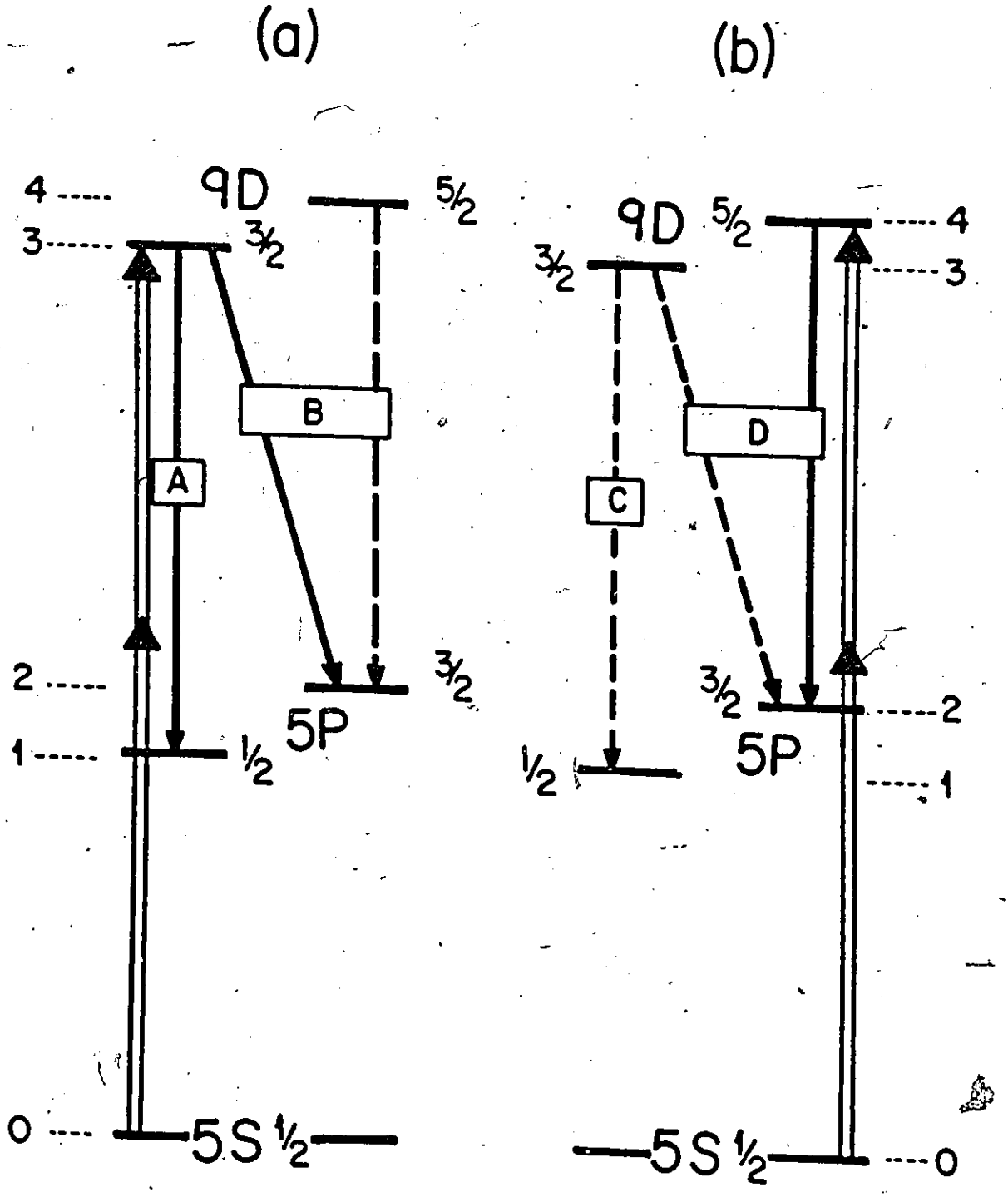

II.2 Excitation and Decay Processes

It is possible to represent the collisional transfer of excitation energy between the fine-structure sub-states of excited Rb atoms by the following equations:

$$Rb(9\ ^2D_{3/2}) + B + \Delta E \leftrightarrow Rb(9\ ^2D_{5/2}) + B \tag{7}$$

$$Rb(9\ ^2D_{3/2}) + Rb(5\ ^2S_{1/2}) + \Delta E \leftrightarrow Rb(9\ ^2D_{5/2}) + Rb(5\ ^2S_{1/2}) \tag{8}$$

where B is the neutral perturber atom and $\Delta E = 0.70 cm^{-1}$ is the fine-structure splitting of the 9 ^{2}D state.

Figure 1 is a partial energy-level diagram showing the processes involved in the excitation and decay of the 9 ^{2}D states. One of the 9 ^{2}D states is selectively excited by two-photon absorption and subsequently decays to a 5 ^{2}P state. The 9 $^2D_{3/2}$ state may decay to either the 5 $^2P_{1/2}$ or 5 $^2P_{3/2}$ states, while the 9 $^2D_{5/2}$ state may only decay to the 5 $^2P_{3/2}$ states. The separation of the two 5 P states, $\Delta E = 237.61 cm^{-1}$, is large enough to be resolved by a monochromator , while the separation

between the 9 D states $\Delta E = 0.70 cm^{-1}$, cannot be resolved. As a result, the fluorescence spectrum is composed of two components. When the 9 $^2D_{3/2}$ state is optically excited (Fig 1-a), component A is the result of direct fluorescence, while B is the result of both the direct and the sensitized fluorescence. Similarly, when the 9 $^2D_{5/2}$ state is optically excited (Fig.1-b), component C is due entirely to sensitized fluorescence, and D is due to both sensitised and direct fluorescence. The wavelengths corrosponding to these transitions are listed in Table 1.

Table 1: Wavelengths Associated with $9^2D \Leftrightarrow 5^2P$ Transitions

Transition	Wavelength Å	Component
$9D_{3/2} \Leftrightarrow 5P_{1/2}$	5196.7	A or C
$9D_{3/2} \Leftrightarrow 5P_{3/2}$	5261.8	B or D
$9D_{5/2} \Leftrightarrow 5P_{3/2}$	5261.5	B or D
$5S_{1/2} \Leftrightarrow 9D_{3/2}$	3142.5	-
$5S_{1/2} \Leftrightarrow 9D_{5/2}$	3142.4	-

If τ_3, τ_4 is defined as the mean lifetimes of the ^2D states, N_o as the density of the perturber, N_i the density of the states where i=1-4 refer to the states

$5\,P_{1/2}$, $5\,P_{3/2}$, $9\,D_{3/2}$, $9\,D_{5/2}$, respectively, then the time-evolution of the population densities of the $9\,D_{3/2}$ and $9\,D_{5/2}$ states can be represented as:

$$\frac{dN_3}{dt} = N_4 N_0 v Q_{43} - N_3\left(\frac{1}{\tau_3} + N_0 v Q_{34} + N_0 v Q_3\right) \qquad (9)$$

$$\frac{dN_4}{dt} = N_3 N_0 v Q_{34} - N_4\left(\frac{1}{\tau_4} + N_0 v Q_{43} + N_0 v Q_4\right) \qquad (10)$$

Q_{34} and Q_{43} are the total thermally averaged cross sections for transfers $9D_{3/2} \Leftrightarrow 9D_{5/2}$ and $9D_{6/2} \Leftrightarrow 9D_{3/2}$ respectively, while Q_3 and Q_4 represent the quenching cross sections for transfer out of the $9^2D_{3/2}$ and the $9^2D_{5/2}$ fine-structure states to all other Rb states; v is the average relative speed of the colliding partners:

$$v = \left(\frac{8kT}{\pi\mu}\right)^{1/2} \qquad (11)$$

and μ is their reduced mass.

Equations (9) and (10) can be integrated over time for the case of time-dependent populations resulting from the use of pulsed excitation, and the ratios of the optically excited populations to collisionally excited populations written as:[18,21]

$$\frac{\langle N_3 \rangle}{\langle N_4 \rangle} = \frac{1}{\tau_4} \frac{1}{Q_{34}} \frac{1}{N_0 v} + \frac{Q_{43} + Q_4}{Q_{34}} \tag{12}$$

$$\frac{\langle N_4 \rangle}{\langle N_3 \rangle} = \frac{1}{\tau_3} \frac{1}{Q_{43}} \frac{1}{N_0 v} + \frac{Q_{34} + Q_3}{Q_{43}} \tag{13}$$

The fluorescence intensity is a product of the population and the Einstein A coefficients[8] and accordingly:

$$\frac{I_{31}}{I_{32}} = \frac{A_{31}}{A_{32}} \tag{14}$$

$$\frac{I_{42}}{I_{32}} = \frac{N_4}{N_3}\frac{A_{42}}{A_{32}} \tag{15}$$

Since the measured intensity ratio of the fluorescence arises from all transitions involved,

$$\frac{I_B}{I_A} = \frac{I_{32}+I_{42}}{I_{31}} \tag{16}$$

or, using eqs. (14) and (15),

$$\frac{\langle N_3\rangle}{\langle N_4\rangle} = \frac{A_{42}}{A_{31}}\left[\frac{I_B}{I_A} - \frac{A_{32}}{A_{31}}\right]^{-1} \tag{17}$$

Similarly:

$$\frac{\langle N_4\rangle}{\langle N_3\rangle} = \frac{A_{31}}{A_{42}}\left[\frac{I_D}{I_C} - \frac{A_{32}}{A_{31}}\right] \tag{18}$$

The collisional cross sections can be connected to the measured fluorescence intensities by substitution of eqs. (17) and (18) into eqs. (12) and (13) respectively. When the 9 $^2D_{3/2}$ state is optically excited:

$$\frac{A_{42}}{A_{31}}\left[\frac{I_B}{I_A}-\frac{A_{32}}{A_{31}}\right]^{-1}=\frac{1}{\tau_4}\frac{1}{Q_{34}}\frac{1}{N_0 v}+\frac{Q_{43}+Q_4}{Q_{34}} \qquad (19)$$

When the 9 $^2D_{5/2}$ state is optically excited:

$$\frac{A_{31}}{A_{42}}\left[\frac{I_D}{I_C}-\frac{A_{32}}{A_{31}}\right]=\frac{1}{\tau_3}\frac{1}{Q_{43}}\frac{1}{N_0 v}+\frac{Q_{34}+Q_3}{Q_{43}} \qquad (20)$$

The ratios I_B/I_A and I_D/I_C are the fluorescence intensity ratios found experimentally.

The Einstein A coefficients were found to be $A_{31}/A_{42}=0.8057$, and $A_{32}/A_{31}=0.2085$, using the relation:[22]

$$\frac{A_{ji}}{A_{mk}} = \frac{f_{ij}}{f_{km}} \frac{\left(\frac{g_m}{g_k}\right)}{\left(\frac{g_j}{g_i}\right)} \frac{\nu_{ij}}{\nu_{km}} \qquad (21)$$

where ν is the spectral frequency associated with the transition, g are the statistical weights, and f are the oscillator strengths.[23]

The density of the ground-state collision partner is given by:

$$N_0\left(cm^{-3}\right) = \frac{0.133416\left(\frac{J}{mTorr}\right)}{k} \frac{P\,(mTorr)}{T\ \ (K)} \qquad (22)$$

Thus using eq. (11) it is possible to write:

$$\frac{1}{N_0 v} = \frac{C\sqrt{T}}{P} \qquad (23)$$

where:

$$C = \left(\frac{\pi k \mu}{8(0.133416)^2}\right)^{1/2} \qquad (24)$$

and T (K) and P (mTorr) are the measured temperatures and pressures respectively.

The lifetimes τ_3 and τ_4 are assumed to be equal. Table 2 lists various values of the lifetimes recently reported in the literature.

Table 2: Lifetimes of 9^2D Rb states

Reference	τ (ns)	Source
Waligorski et.al.[24]	618±30	Experimental
Gounand et.al.[25]	565±120	" "
Marek and Munster[26]	568±35	" "
Lindgärd and Neilsen[27]	722.8	Theoretical
Grudzev and Denisov[28]	750	" "
Theodosiou[29] J=3/2	625.98	" "
J=5/2	606.96	" "

Waligorski's[24] value of 618 ns was used because of its reasonable agreement with all of the experimental values and its agreement, within error, with the theoretical values of Theodosiou[29].

III. THE APPARATUS AND EXPERIMENTAL PROCEDURE

The excitation of Rb from the 5 $S_{1/2}$ ground-state to one of the 9 ^2D sub-states was accomplished by two-photon absorption of laser light at wavelength 6284Å, corresponding to one-half the energy separation of the two states. The laser output, tuned to selectively excite one of the sub-states, was made incident on Rb vapour or a mixture of Rb vapour and a buffer gas contained in a Pyrex fluorescence cell.

The fluorescence cell was mounted at the centre of an oven fitted with three windows: two in the beam path, coincident with the end walls of the cell, and a third in the side-wall. The window in the side of the cell allowed the fluorescence, emitted perpendicular to the incoming beam, to be focused onto the slit of a monochromator which resolved it into its spectral components of wavelengths 5197 Å and 5261 Å. After emerging from the monochromator's two exit slits, the relative intensities of the two components were measured and recorded using the amplification-discrimination electronics. The simultaneous measurement of both the sensitized and direct components of the fluorescence

minimized the effects of fluctuations in laser intensity and side-arm temperature, or pressure variations from run to run.

Monitoring of the vapour and buffer gas pressures and cell temperatures made it possible to plot the fluorescence intensity ratios against the vapour or buffer gas densities to obtain the thermally averaged cross sections.

Figure 2: Schematic diagram of the apparatus: FP is the Fabry-Perot etalon; F_C is the colour filter; M is the monochromator; PM are the photo-multipliers; PC is the photon counter; P is the printer, and D is the photo-diode.

Figure 2

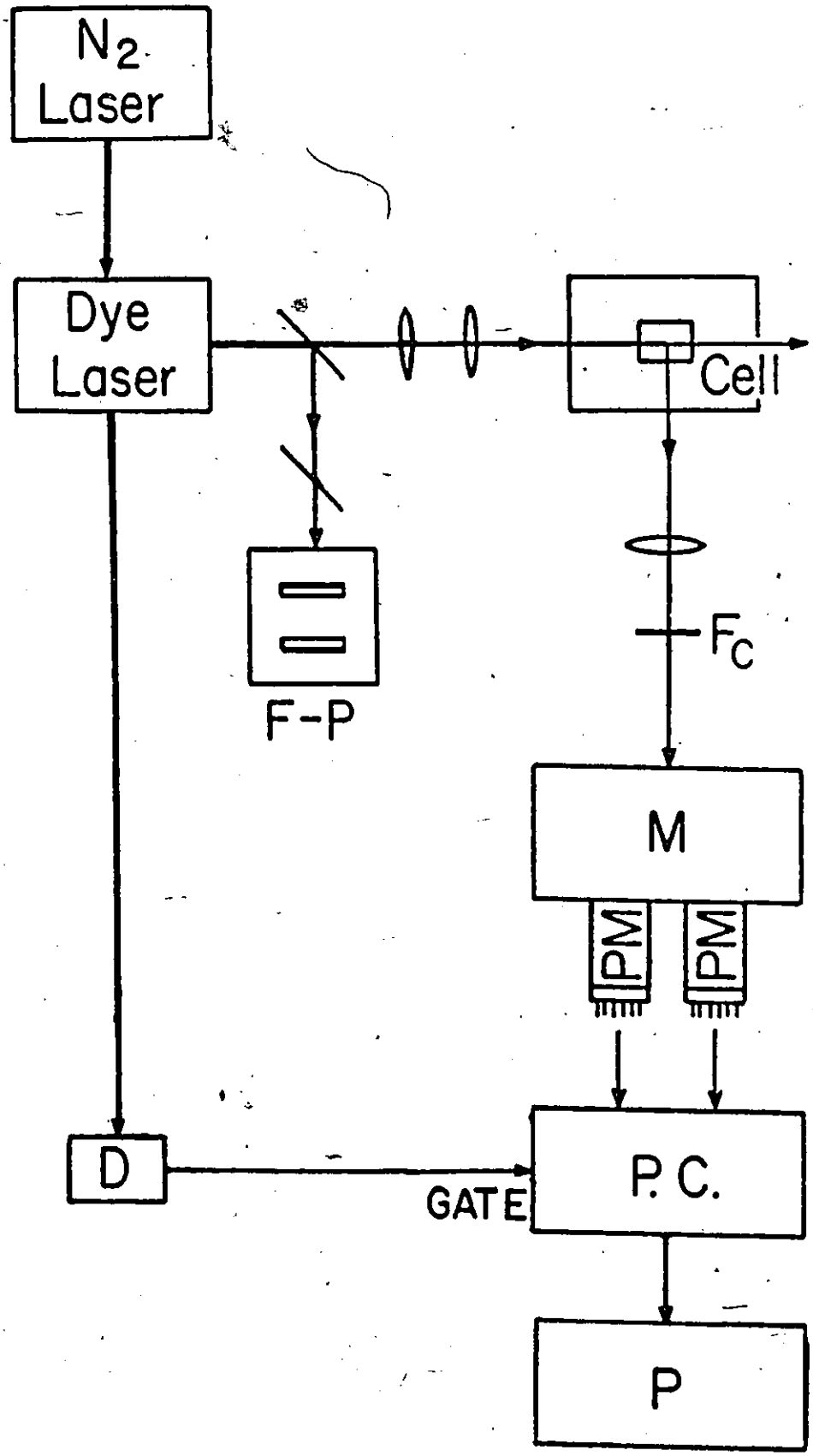

III.1 Description of the Apparatus

A schematic diagram of the apparatus is shown in Fig. 2. The radiation emitted by an N_2 laser-pumped dye laser was weakly focussed into the fluorescence cell mounted in an oven and containing either pure Rb vapour or a mixture of Rb vapour and a noble gas. The resulting fluorescence, emitted perpendicular to the direction of the incoming laser light, was analyzed with a monochromator, detected with a photomultiplier and registered with a photon counter.

A N_2 laser, with a repetition rate of 18 Hz and pulse length of approximately 10 ns, was used to pump an in-house built dye laser whose configuration was based on the Littman double-grating design.[30] The light from the dye laser oscillator was loosely focused into a second dye cell which amplified the laser radiation. Both dye cells were magnetically stirred and both contained a 5×10^{-3}M solution of Rhodamine 640 (R640) in ethanol. Two-photon excitation of the 9 ^2D states takes place at about 6285 Å, within the R640 effective output range of 6200 Å - 6500 Å.

The cylindrical pyrex fluorescence cell was 4 cm long and 2.5 cm in diameter. A 7 cm long and 1 cm in

diameter side-arm extended downward from the fluorescence cell and acted as a Rb reservoir. The cell and reservoir were connected by a greaseless stopcock to the vacuum and gas-delivery system. This set-up ensured a minimal loss of Rb while still allowing for the effective pressurization or evacuation of the cell.

The Rb side-arm, contained in a separate jacket, was heated with silicon oil circulated in a copper tube from an ultrathermostat. The oil temperature was controlled separately from the main oven which was heated electrically.

The temperatures of the cell and side arm were monitored with fourteen copper-constantan thermocouples. The temperatures were recorded and monitored on a strip-chart recorder (Hewlett-Packard 7101B).

The fluorescence emitted from the cell was focused through a colour cut-off edge filter, onto the monochromator slit. The monochromator was fitted with a flat 1200 1/mm diffraction grating and two exit slits which allowed for the simultaneous detection of both the 5197 Å and the 5262 Å components. At each exit slit the fluorescence was detected with a thermoelectrically cooled photomultiplier (RCA C31034) whose signal was amplified with a preamplifier (built in house), and

conveyed to an amplifier-discriminator (Ortec 9302) to be registered with a photon counter (Ortec 9315).

The pressure of the system was monitored using a capacitance manometer (MKS Baratron) and a convectron vacuum gauge (Granville-Phillips Series 275) calibrated against the capacitance manometer.

The Rb metal, supplied by Metron Inc. of Allamuchy, NJ.,was of 99.9% nominal purity and had been previously redistilled. It was distilled, under vacuum, into the side-arm reservoir of the baked-out cell. The buffer gases, supplied by Union Carbide Linde Gas Products, were of research grade.

III.2 Experimental Procedure

Before starting an experimental run, the system was baked at 480 K for several hours and pumped down to $1x10^{-7}$ Torr. It was then flushed with the buffer gas to be used and again pumped down to $1x10^{-7}$ Torr. Between each set of measurements the system was evacuated to remove any gaseous impurities that may have desorbed from the cell walls. The cell temperature was maintained

approximately 40 K to 85 K above that of the side-arm to avoid condensation of Rb vapour on the cell windows.

During the experimental runs with Rb and the buffer gases, the side-arm temperature was kept at 353 K and remained constant to within ±0.5 K over each experimental run. During the experiment with pure Rb the side-arm temperatures ranged from 378 K to 458 K, which corresponded to pressures from 0.26 mTorr to 20.16 mTorr respectively. The pressure in the cell was calculated from the lowest side arm temperature, using the relation:[31]

$$\log P = 15.88253 - \frac{4529.635}{T} + 5.8663 \times 10^{-4} T - 2.99138 \log T \qquad (25)$$

where the pressure P is given in Torr and the temperature T in Kelvin.

The buffer gas pressure was varied from 3.3 mTorr to 268.0 mTorr depending on the gas and the sensitivity of the fluorescence to changes in the pressure. Pressures below 3 mTorr were difficult to maintain mainly because of outgassing from the cell walls.

The photon counter was gated by pulses from a photodiode which was triggered by the dye laser. The gating pulse turned on the counting system for a period approximately equal to ten lifetimes of the excited state. Thus it was possible to count most of the light emitted in the solid angle of detection while at the same time minimizing the noise. Since the photon counter could distinguish between pulses as close as 10 ns apart, and the count-rate never exceeded 0.02 photons per 10 ns of active time, the effects of pile-up or overlap of photons were negligible.

The spectral width of the dye laser light, monitored with a Fabry-Perot etalon (Quanta-Ray FPA1) was found to be about 6 GHz (0.19 cm-1), over 3 times smaller than the 9 D fine-structure separation of 21.0 GHz (0.70 cm-1).

Before each experimental run the cell was evacuated to its base pressure of 1×10^{-7} Torr, and the side arm heated to 353 K or a Rb pressure of 4×10^{-5} Torr. The laser was detuned and the background determined. To ensure the selectivity of the excitation process the tuning was then adjusted to maximize the output for the directly excited fluorescence component while maintaining the collisionally excited component near the background

level. The buffer gas was then admitted and the system allowed to stabilize. The count rate of one channel was taken over a three minute interval using the photon counter's internal timer and the output recorded on the printer. The photon counter was then set to accept a pre-set number of counts in one channel.

As a result of the low vapour pressures used in this experiment, Doppler broadening was the predominant line broadening mechanism. The Doppler-broadened line width was given by:

$$\Delta\nu = \nu\sqrt{\frac{8kT\ln 2}{mc^2}} \qquad (26)$$

where ν is the frequency of the spectral line. For the $9\ ^2D$ states this gives a single atomic absorption line width of less than 0.8 GHz. Because two-photon excitation was used in this experiment the effective spectral width of the dye-laser light was 12 GHz, which exceeded the width of the absorption lines, thus ensuring that the sub-state was properly excited.

The relative sensitivities of each photomultiplier

tube to the two fluorescence components was measured using a Rb spectral lamp. It was found that for both photomultiplier tubes the sensitivity ratio of the 5267 Å component to the 5197 Å component was 0.55±0.06. The inter-calibration between the two detection-amplification channels was checked before each run and the ratio recorded. The product of the ratios of the relative sensitivities, inter-calibration, and the ratio of transmissivity for colour cut-off filter was used to scale the collected data.

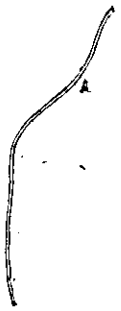

IV. RESULTS AND DISCUSSION

Equations (19) and (20) for the density of states can be rewritten in the form:

$$\frac{A_{42}}{A_{31}}\left[\frac{I_B}{I_A}-\frac{A_{32}}{A_{31}}\right]^{-1}\frac{\tau P}{C\sqrt{T}}=\frac{Q_{43}+Q_4}{Q_{34}}\frac{\tau P}{C\sqrt{T}}+\frac{1}{Q_{34}} \tag{27}$$

$$\frac{A_{31}}{A_{42}}\left[\frac{I_D}{I_C}-\frac{A_{32}}{A_{31}}\right]\frac{\tau P}{C\sqrt{T}}=\frac{Q_{34}+Q_3}{Q_{43}}\frac{\tau P}{C\sqrt{T}}+\frac{1}{Q_{43}} \tag{28}$$

where C is given by eq.(24), P is the pressure in the cell in mTorr, and T is the cell temperature in Kelvin. In the experiment with pure Rb vapour, P was the Rb vapour pressure which varied with T. In the Rb-buffer gas experiment P was the buffer gas pressure and T remained constant.

Plots of the left-hand sides of eq. (27) and (28) against $\tau P/C\sqrt{T}$ are expected to be linear. The inverse intercepts yield the cross sections Q_{34} and Q_{43}, while the values for the effective quenching cross sections Q_3 and Q_4 can be found from the slopes. The experimental

data are shown in Figs. 3-7 and the resulting cross sections are listed in Tables 3-8. An error of ±35% has been assigned to the values Q_{34} and Q_{43}. The uncertainty associated with the values Q_3 and Q_4 was very large, owing to their calculation from Q_{34} and Q_{43} and they can, at best be considered to be accurate within an order of magnitude.

The main source of error, in all cases, is in the calibration sensitivity of the two counting channels; in the experiments with pure Rb there is the additional uncertainty in the determination of the Rb pressure from the side-arm temperature. Smaller errors were associated with the mean lifetime (Table 2), and the calculated Einstein A coefficients.

Varying the intensity of the exciting laser radiation produced no measurable change in the ratio of the sensitized to direct fluorescence, confirming past conclusions that photoionization was negligible at the prevailing laser powers.[8]

The Rb vapour pressure was sufficiently low, (4×10^{-5} Torr during Rb-noble gas runs), that the effect of collisions with Rb_2 molecules and three-body collisions could be neglected. The contribution of residual Rb^*-Rb collisions to the Rb-noble gas cross

sections was calculated to be less than 1% and could thus be considered negligible.

Data for cell gas pressures of less than 3 mTorr was rejected because of the large uncertainty in the measured pressures. This sensitivity at low pressures was particularly noticeable when the 9 $^2D_{3/2}$ state was optically excited, and is a result, in part, of the mixing of the sensitized and direct fluorescent components. In order to determine the sensitized fluorescence intensity with adequate accuracy, it must be of comparable intensity to the direct component.[8] This can only be achieved above a certain threshold pressure, below which the data becomes sensitive to the calibration of the counting system and small errors are magnified into considerable scatter of the data points.

The results of the Rb*-Rb fine-structure mixing collisions are shown in Fig. 3, and are listed in Table 3 together with other previously reported values. In the absence of theoretical calculations, the Rb*-Rb cross sections are compared with the geometrical cross section.

The large Rb*-Rb cross sections, were expected given that the quasi-free nature of the valence electron of the excited Rb atom is influenced by the long-range dipole-dipole interaction between the alkali atoms.[14,32]

The Q_{34} value obtained in this experiment agrees within error with the geometrical cross section calculated for the 9 D state, as well as with the values obtained by Gounand et. al..[33] The Q_{43} cross section agrees within an order of magnitude with the value obtained by Parker et. al..[34] The discrepancy between these two results could arise, in part, from an under-estimate of the Rb vapour density on the part of Parker et.al., since the cross sections reported by this group were consistently smaller than those measured in our laboratory.

The experimental data for 9 ^{2}D fine-structure mixing induced in collision with the noble gases is shown in Figs. 4-7 and the cross sections are listed in Tables 4 - 7. All the graphs exhibit the expected linearity. As anticipated, the cross sections for Rb*-noble gas collisions are smaller than those for Rb*-Rb collisions by more than one order of magnitude.

The fine-structure mixing cross sections can be ordered from He to Kr, with a minimum at Ne. In Fig.8 the fine-structure mixing cross sections are compared with the corrosponding total cross section for electron scattering [16] which demonstrates a similar trend. This trend is also apparent in the n=7,8 cross sections as can

be seen in Fig.9.[35] The velocity-dependent electron cross sections were calculated for the 9 D orbital velocities of the excited Rb atom.

The size of the cross sections should tend to increase with increasing relative velocity of the colliding partners.[8] This is due to the thermal equilibrium condition under which these measurements were taken, limiting the collisions to adiabatic changes.[13,16] That is to say, that the relative velocity of the colliding partners is less than the orbital velocity of the 9 D electron. Thus the cross sections would tend to decrease with increasing mass of the noble gas perturber.[8]

A second effect to which the cross sections are subject, is the increase in polarizability of the buffer gases from He to Kr. Thus the range of the interactions between the ionic core of the excited Rb atom and the perturber would increase since the long-range electrostatic interactions are proportional to the polarizabilities and the atoms with larger polarizability should produce larger cross sections, a trend opposite to that expected from increasing relative velocity of the atoms.

A third factor affecting the Rb-noble gas cross

section was the interaction of the perturber with the valence electron of the excited Rb atom. If the Rb valence electron is considered to be quasi-free, the interaction should be a minimum for collisions with Ne and Ar.[8] The quasi-free model is applicable to highly excited states rather than the intermediate states such as the 9 D states which I am considering and is, therefore, of limited applicability to the relative ordering of the cross sections.

It is not obvious to what extent each of these mechanisms influences the relative ordering of the fine-structure mixing cross sections. However, since this ordering trend has been observed in several similar studies[2,8,35,36] it is likely that a similar mechanism governs the collisional processes for all intermediate Rydberg states.

In comparing the Rb*-noble gas cross sections for the 9 D with those for other n states (Table 5 - 8), it should be noted that, for intermediate n values, the collision cross sections tend to rise with n to a maximum and then gradually decrease as n increases.[33,37] The position of this maximum depends on the buffer gas. The measured cross sections for collisions of Rb with Ar and Kr show this increase of Q_{34} with n while the Rb-He and

Rb-Ne cross sections remain constant for n=7-9 within the stated limits of error.

This trend of the fine-structure mixing cross sections was predicted by a semi-classical theory of Sirko and Rosinski[16] (Fig. 10) which is similar in approach to that proposed for l-mixing by de Prunelé and Pascale.[13] The values which I obtained for Rb*-Ne and Rb*-Kr cross sections fall between the upper and lower bounds predicted by the model, while those for Rb*-Ar and Rb*-He agree within error.

The internal consistency of the data can be checked using the principle of detailed balancing which predicts the ratio of the fine-structure mixing cross sections:[18,38]

$$\frac{Q_{34}}{Q_{43}} = \frac{g_4}{g_3}\exp\left[\frac{-\Delta E}{kT}\right] \qquad (29)$$

where $g_{3,4}=(2J + 1)$, are the statistical weights equal to 4 and 6 for g_3 and g_4, respectively, $\Delta E = 0.70 cm^{-1}$ is the 9^2D fine-structure splitting and T=353 K. The predicted

value is $Q_{34}/Q_{43}=1.50$ for the 9 ^2D cross sections. The ratios of the measured cross sections agree with the predicted ratio within the stated limits of error, indicating the degree of internal consistency of the data.

Figure 3: A plot of left sides of eqn. (27) and (28) against $\tau P/C\sqrt{T}$ for Rb^*-Rb. Error bars are representative of error over the range of gas pressures.

Figure 3

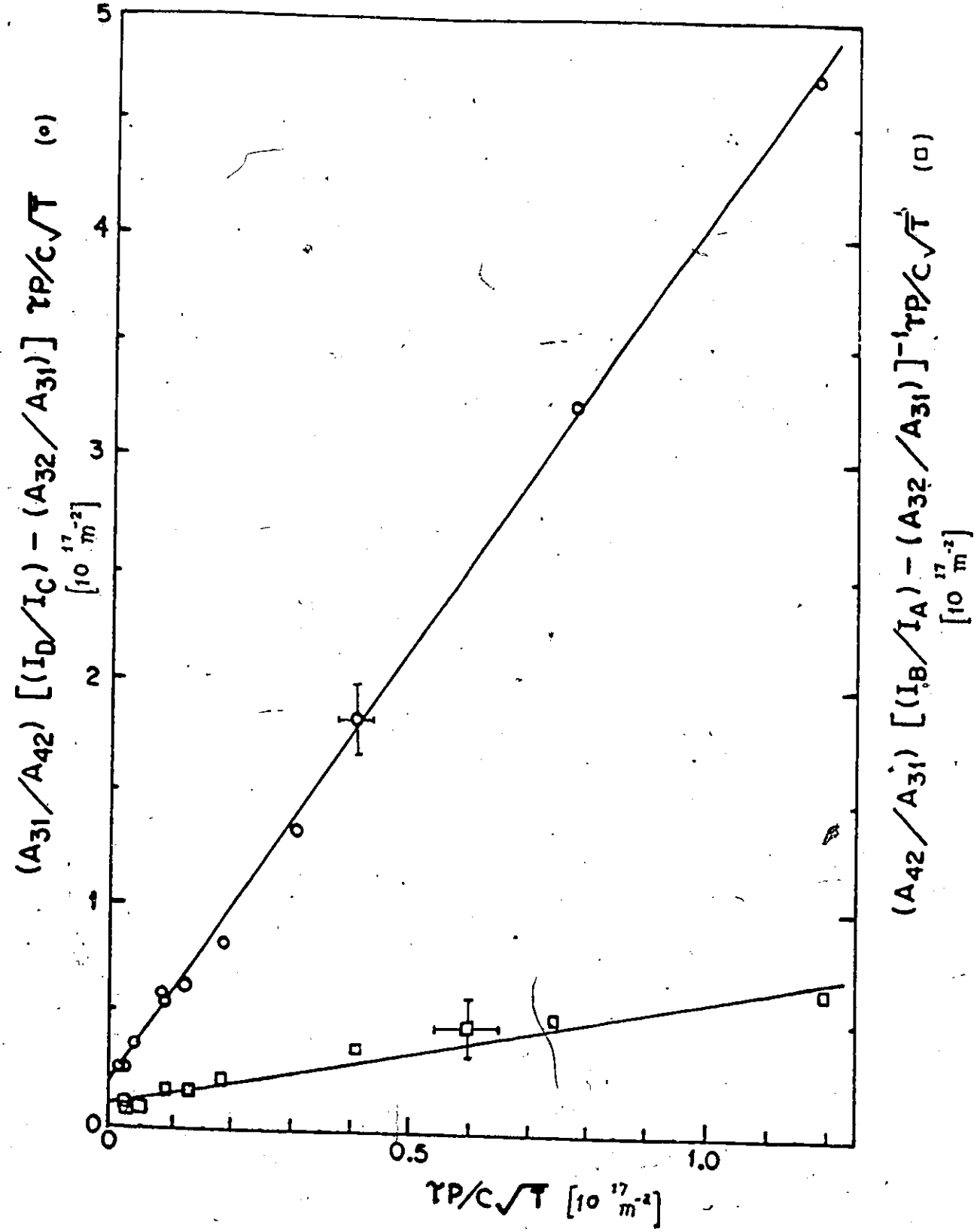
5
4
3
2
1
0
0
0.5
1.0
$(A_{31}/A_{42})\,[(I_D/I_C)-(A_{32}/A_{31})]\,\gamma P/C\sqrt{T}$ (○)
$[10^{17}\,m^{-2}]$
$(A_{42}/A_{31})\,[(I_B/I_A)-(A_{32}/A_{31})]^{-1}\gamma P/C\sqrt{T}$ (□)
$[10^{17}\,m^{-2}]$
$\gamma P/C\sqrt{T}$ $[10^{17}\,m^{-2}]$

Table 3: $n^2D_{3/2} \leftrightarrow n^2D_{5/2}$ Fine-structure Mixing Cross Sections for Rb*-Rb Collisions
($10^{-14} cm^2$)

Collisional Partners	Q_{34}	Q_{43}	$\frac{Q_{34}}{Q_{43}}$	n^*	σ_g	$\Delta E(cm^{-1})$	Ref
$Rb(6D) \rightarrow Rb(5S)$	17.3±3.5	11.6±2.3	1.49	4.68	8.90	2.26	8
$Rb(7D) \rightarrow Rb(5S)$	30±5	18±3	1.65	5.67	20.0	1.51	8
$Rb(8D) \rightarrow Rb(5S)$	43.1±8.6	28.5±8.6	1.51	6.7	40.0	1.01	8
$Rb(9D) \rightarrow Rb(5S)$	91±32 65±20 70±30 --	62±22 -- -- 26.5±5.0	1.61 -- -- --	7.66	71.3	0.70	this work 32 33 34

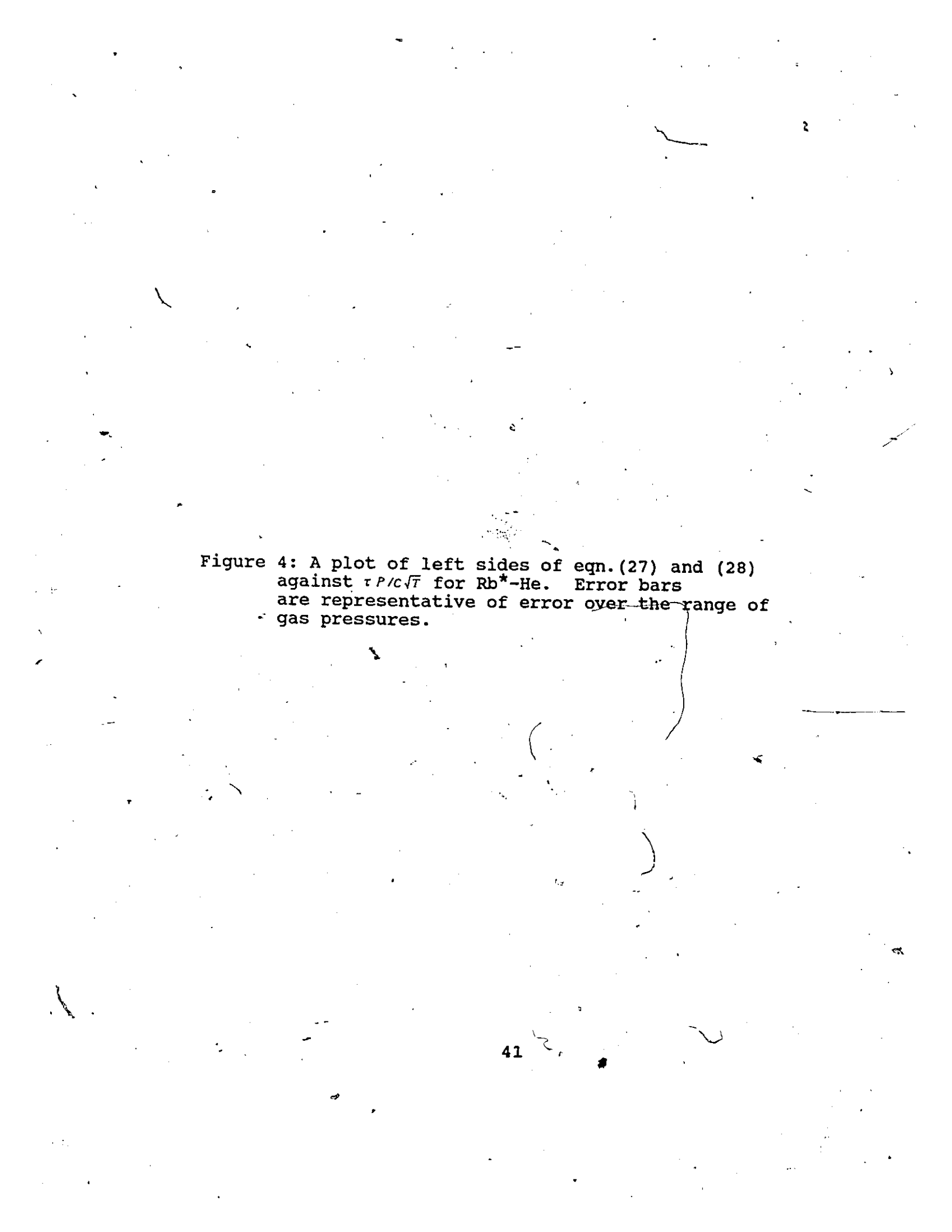

Figure 4: A plot of left sides of eqn.(27) and (28) against $\tau P/c\sqrt{T}$ for Rb*-He. Error bars are representative of error over the range of gas pressures.

Figure 4

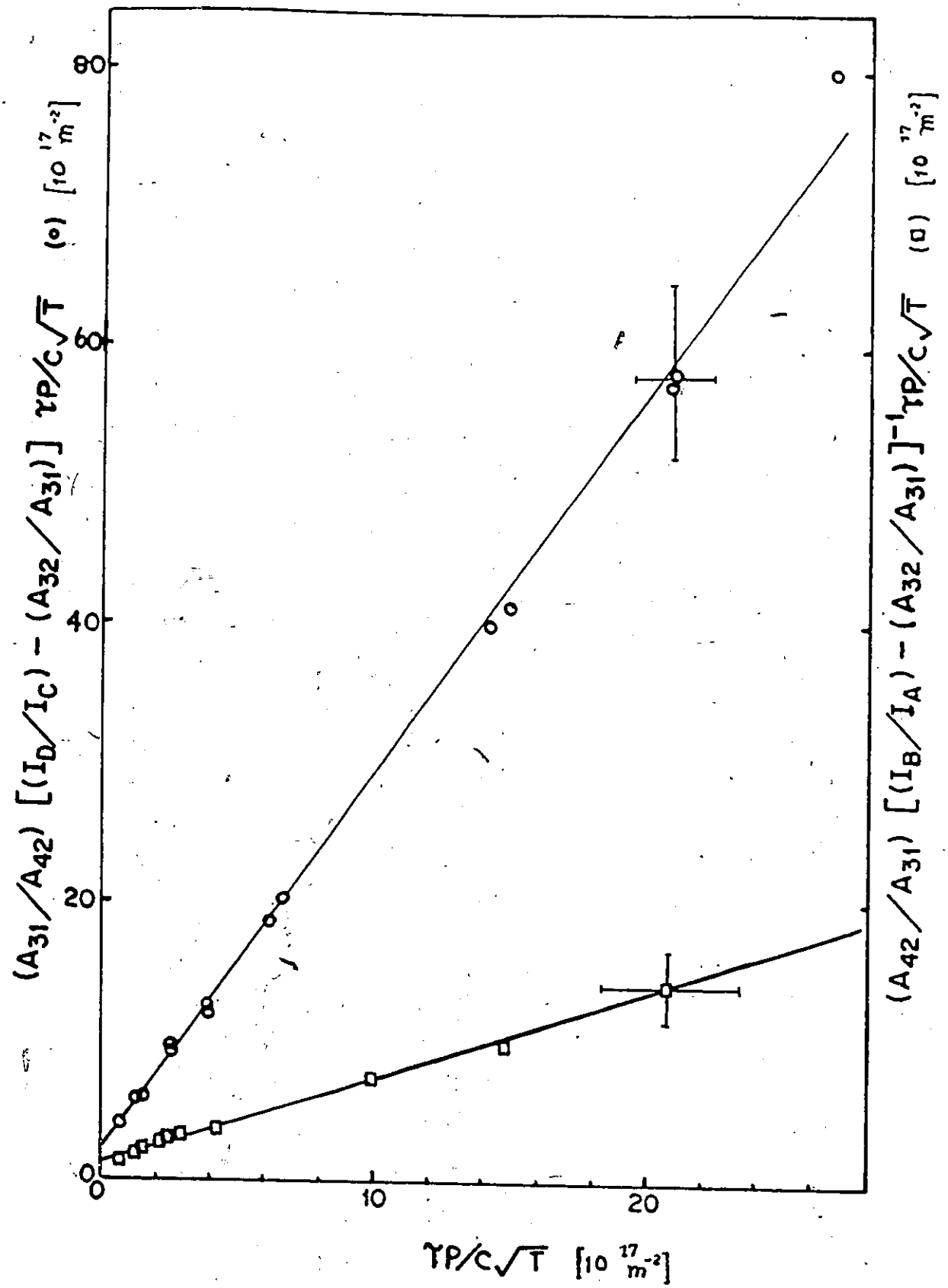
80
60
40
20
0
0
10
20
$(A_{31}/A_{42})\,[(I_D/I_C) - (A_{32}/A_{31})]\;\gamma P/c\sqrt{T}$ (o) $[10^{17}\,m^{-2}]$
$(A_{42}/A_{31})\,[(I_B/I_A) - (A_{32}/A_{31})]^{-1}\gamma P/c\sqrt{T}$ (□) $[10^{17}\,m^{-2}]$
$\gamma P/c\sqrt{T}$ $[10^{17}\,m^{-2}]$

Figure 5: A plot of left sides of eqn.(27) and (28) against $\tau P/C\sqrt{T}$ for Rb*-Ne. Error bars are representative of error over the range of gas pressures.

Figure 5

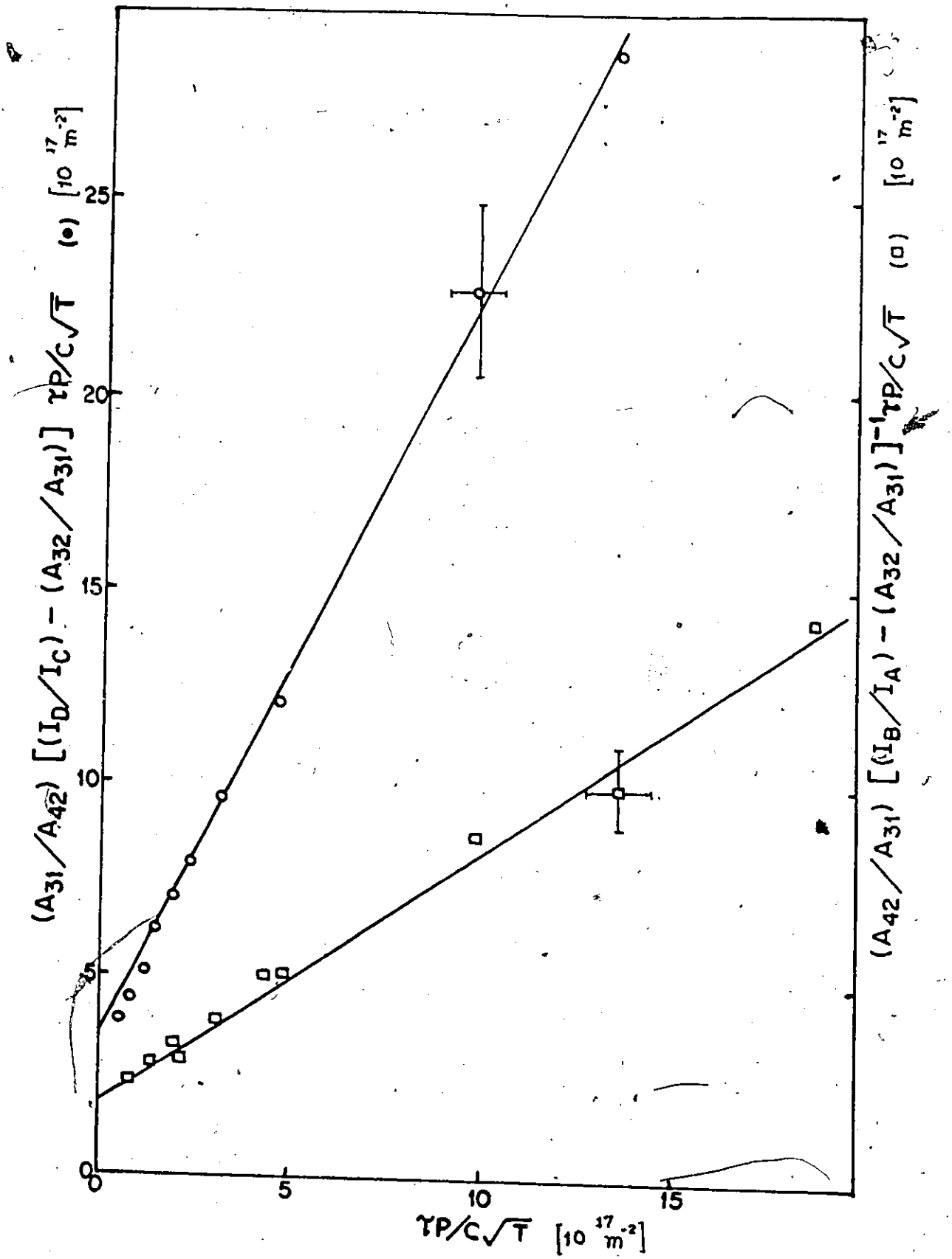
(A31/A42) [(ID/IC) − (A32/A31)] τP/C√T (•) [10^17 m^-2]
(A42/A31) [(IB/IA) − (A32/A31)]^-1 τP/C√T (□) [10^17 m^-2]
τP/C√T [10^17 m^-2]
0
5
10
15
20
25

Figure 6: A plot of left sides of eqn.(27) and (28) against $\tau P/c\sqrt{T}$ for Rb*-Ar. Error bars are representative of error over the range of gas pressures.

Figure 6

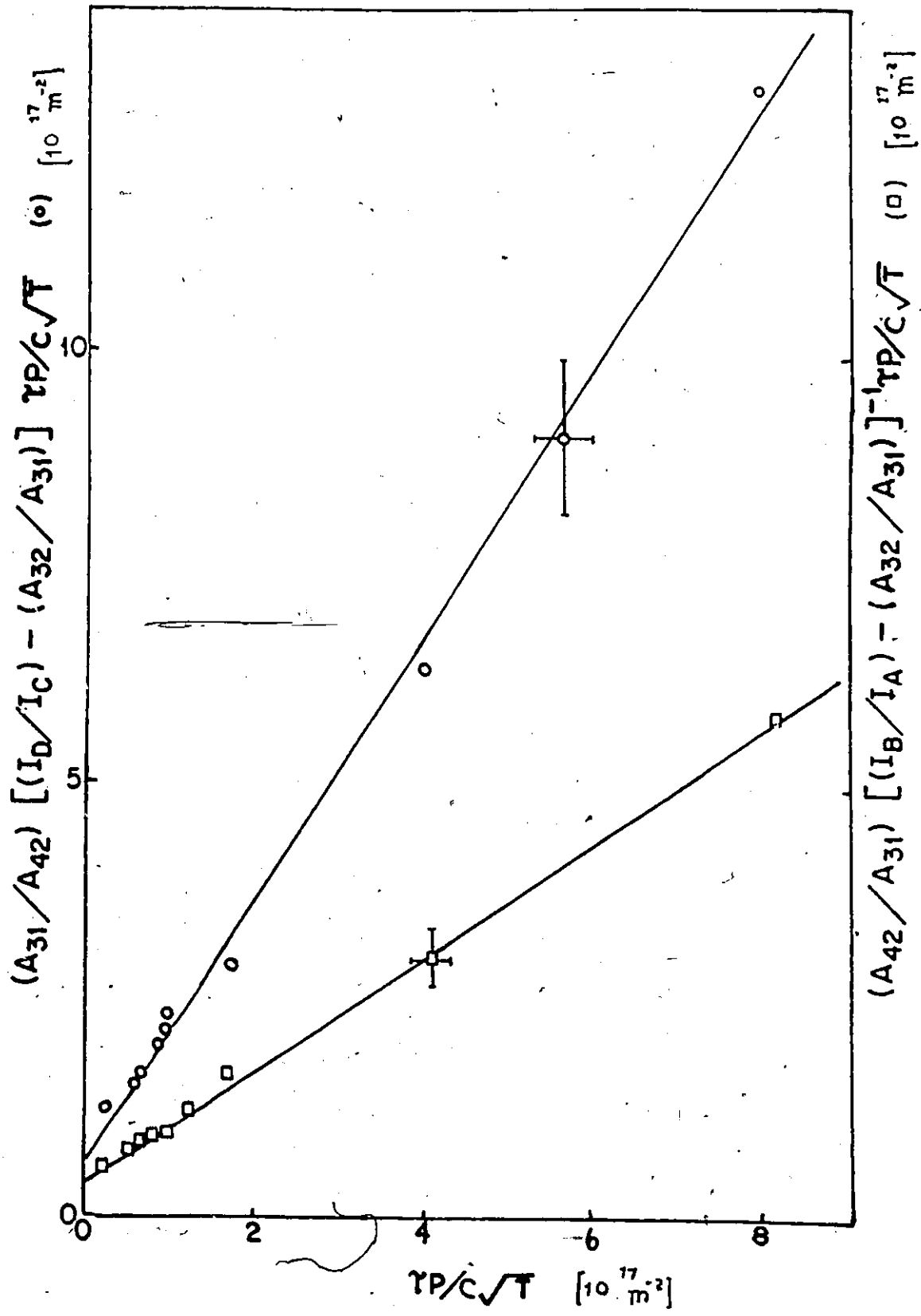
(A31/A42) [(ID/IC) - (A32/A31)] γP/C√T (○) [10^17 m^-2]
(A42/A31) [(IB/IA) - (A32/A31)]^-1 γP/C√T (□) [10^17 m^-2]
γP/C√T [10^17 m^-2]
0
2
4
6
8
10
5

Figure 7: A plot of left sides of eqn.(27) and (28) against $\tau P/C\sqrt{T}$ for Rb*-Kr. Error bars are representative of error over the range of gas pressures.

Figure 7

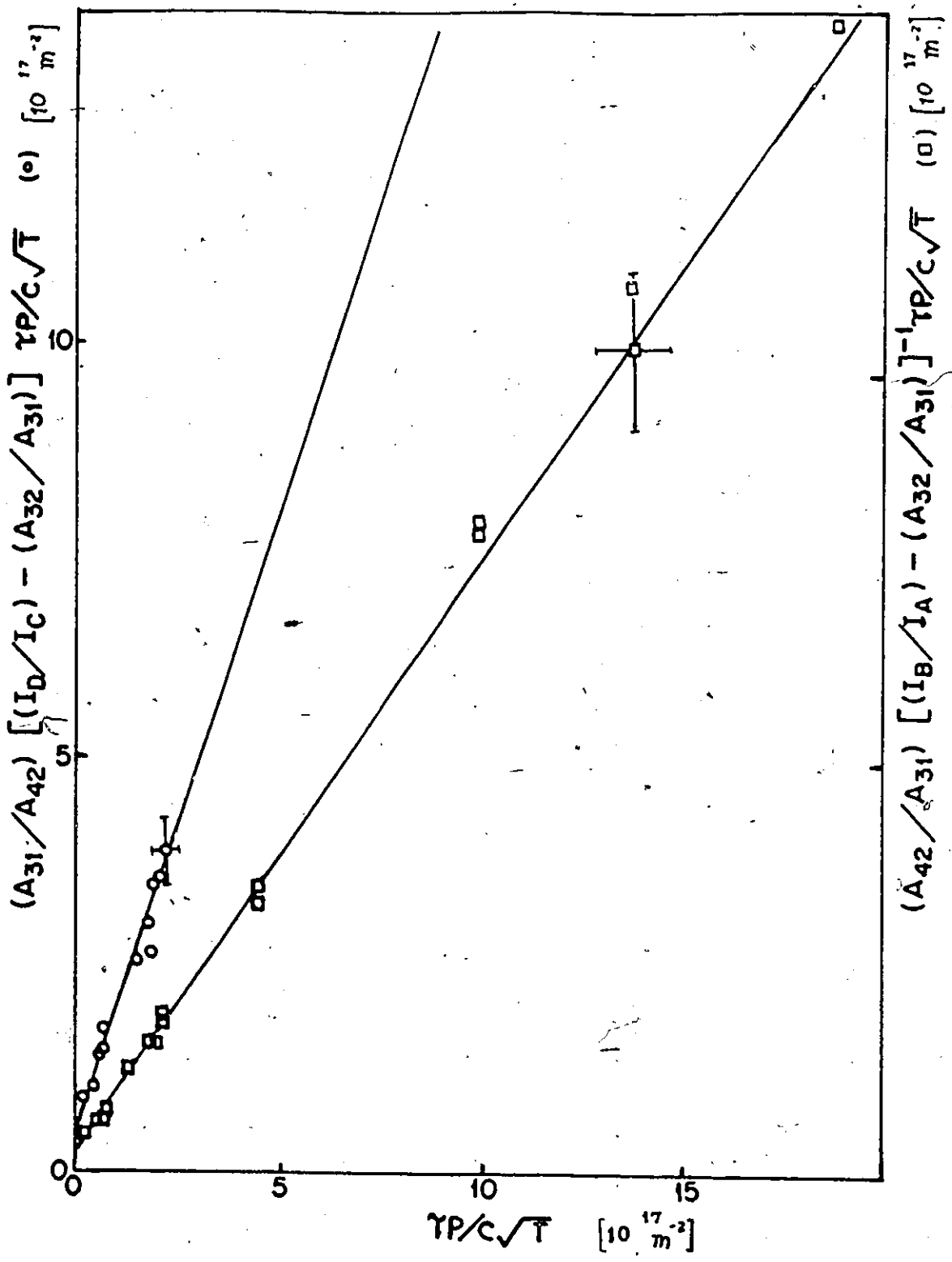
$(A_{31}/A_{42})\,[(I_D/I_C) - (A_{32}/A_{31})]\;\gamma P/c\sqrt{T}$ (o) $[10^{17}\,m^{-2}]$
$(A_{42}/A_{31})\,[(I_B/I_A) - (A_{32}/A_{31})]^{-1}\gamma P/c\sqrt{T}$ (□) $[10^{17}\,m^{-2}]$
$\gamma P/c\sqrt{T}$ $[10^{17}\,m^{-2}]$
0
5
10
15

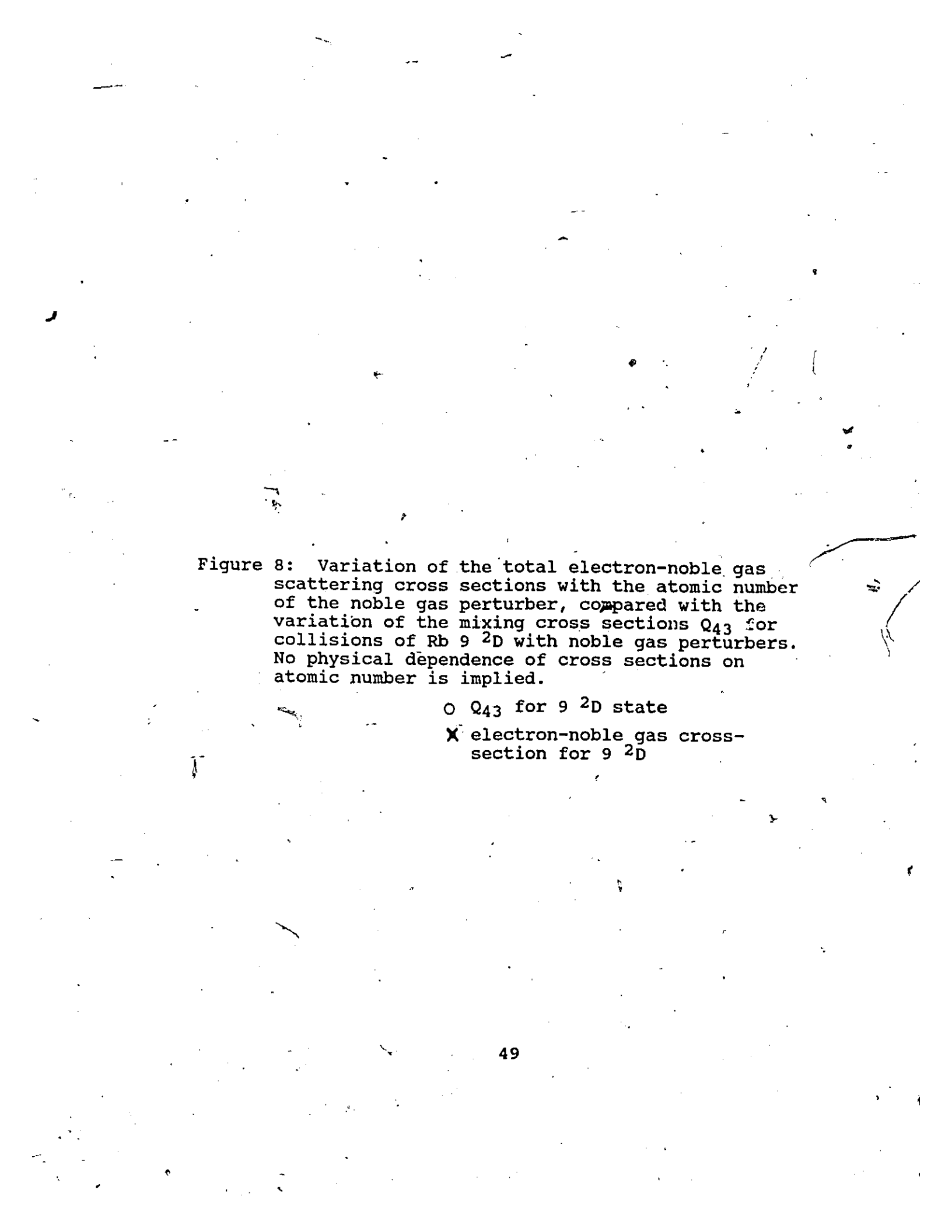

Figure 8: Variation of the total electron-noble gas scattering cross sections with the atomic number of the noble gas perturber, compared with the variation of the mixing cross sections Q_{43} for collisions of Rb 9 ^2D with noble gas perturbers. No physical dependence of cross sections on atomic number is implied.

○ Q_{43} for 9 ^2D state

✕ electron-noble gas cross-section for 9 ^2D

Figure 8

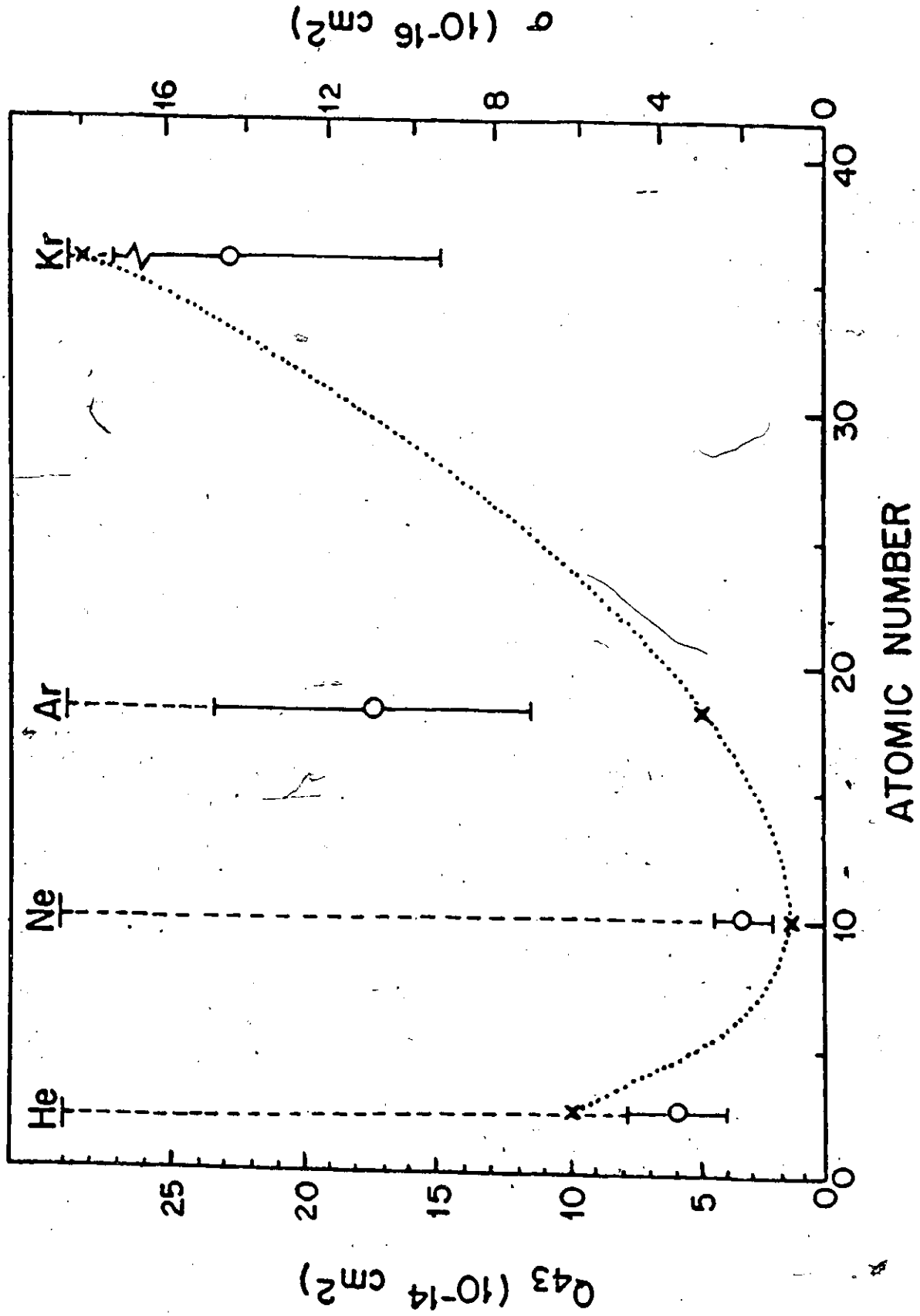
σ (10⁻¹⁶ cm²)
16
12
8
4
0
Kr
Ar
Ne
He
40
30
20
10
0
ATOMIC NUMBER
25
20
15
10
5
0
Q43 (10⁻¹⁴ cm²)

Figure 9: Variation of elastic-electron scattering cross section with the atomic number of the noble gas perturber compared with the variation of the mixing cross section Q_{43} for collisions with noble gas perturber for Rb 7 ^2D and 8 ^2D.

▲ Q_{43} for 7 ^2D

△ corresponding electron scattering cross section for the 7 ^2D state

● Q_{43} for 8 ^2D

○ corresponding electron scattering cross section for the 8 ^2D state

Figure 9

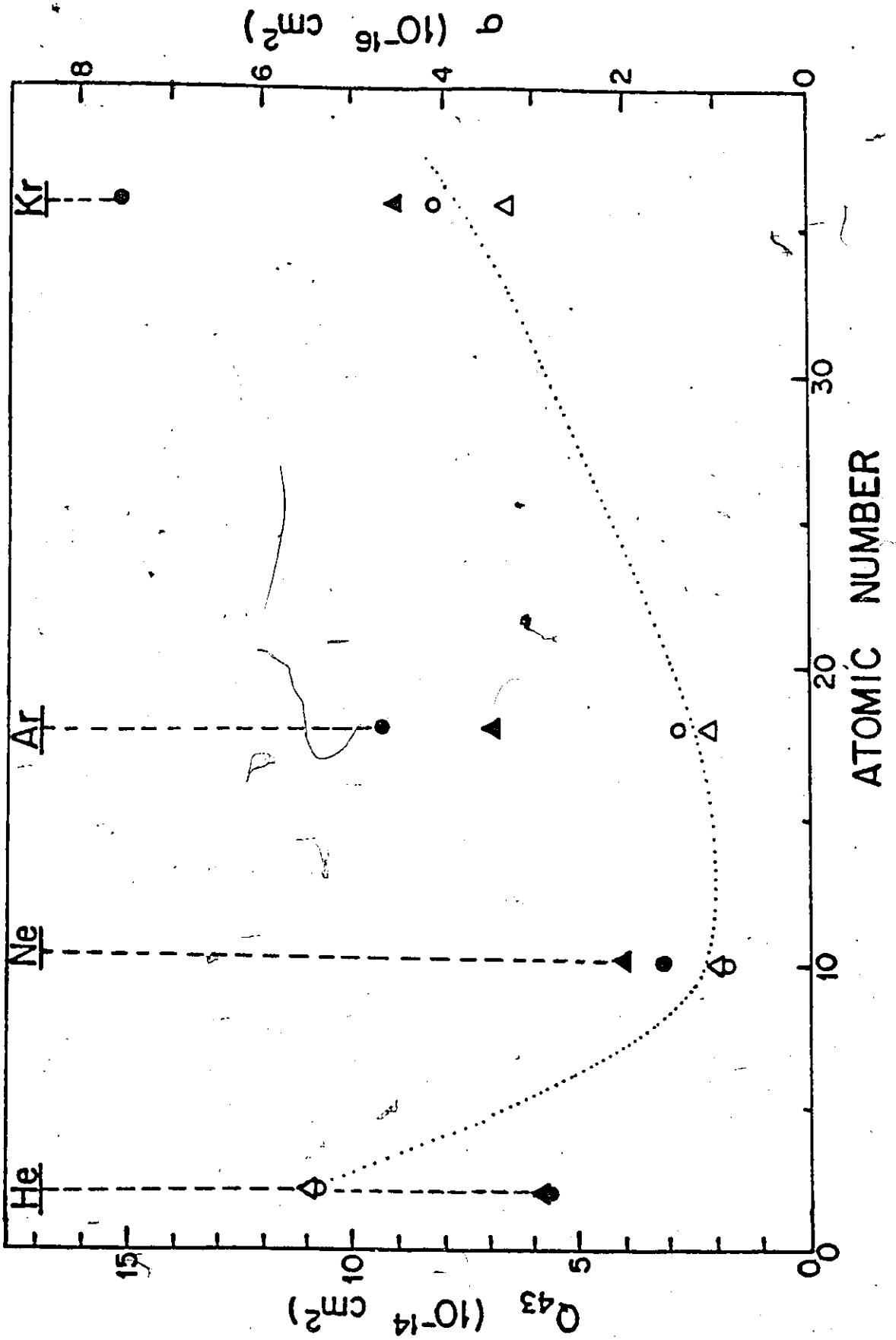
σ (10⁻¹⁶ cm²)
0
2
4
6
8
Kr
Ar
Ne
He
ATOMIC NUMBER
0
10
20
30
Q43 (10⁻¹⁴ cm²)
0
5
10
15

Figure 10: Fine-structure mixing cross sections for $9^2D_{3/2} \leftrightarrow 9^2D_{5/2}$ mixing induced in collisions with noble gases. The curves show upper and lower limits predicted at T_{cell}=380K by the theory proposed by Sirko and Rosinski.[16]

Experimental points:
- ○ Supronowicz[35] (T_{cell}=380K)
- ✕ Hugon et.al.[6] (T_{cell}=520K)
- □ this experiment (T_{cell}=353K)

Figure 10

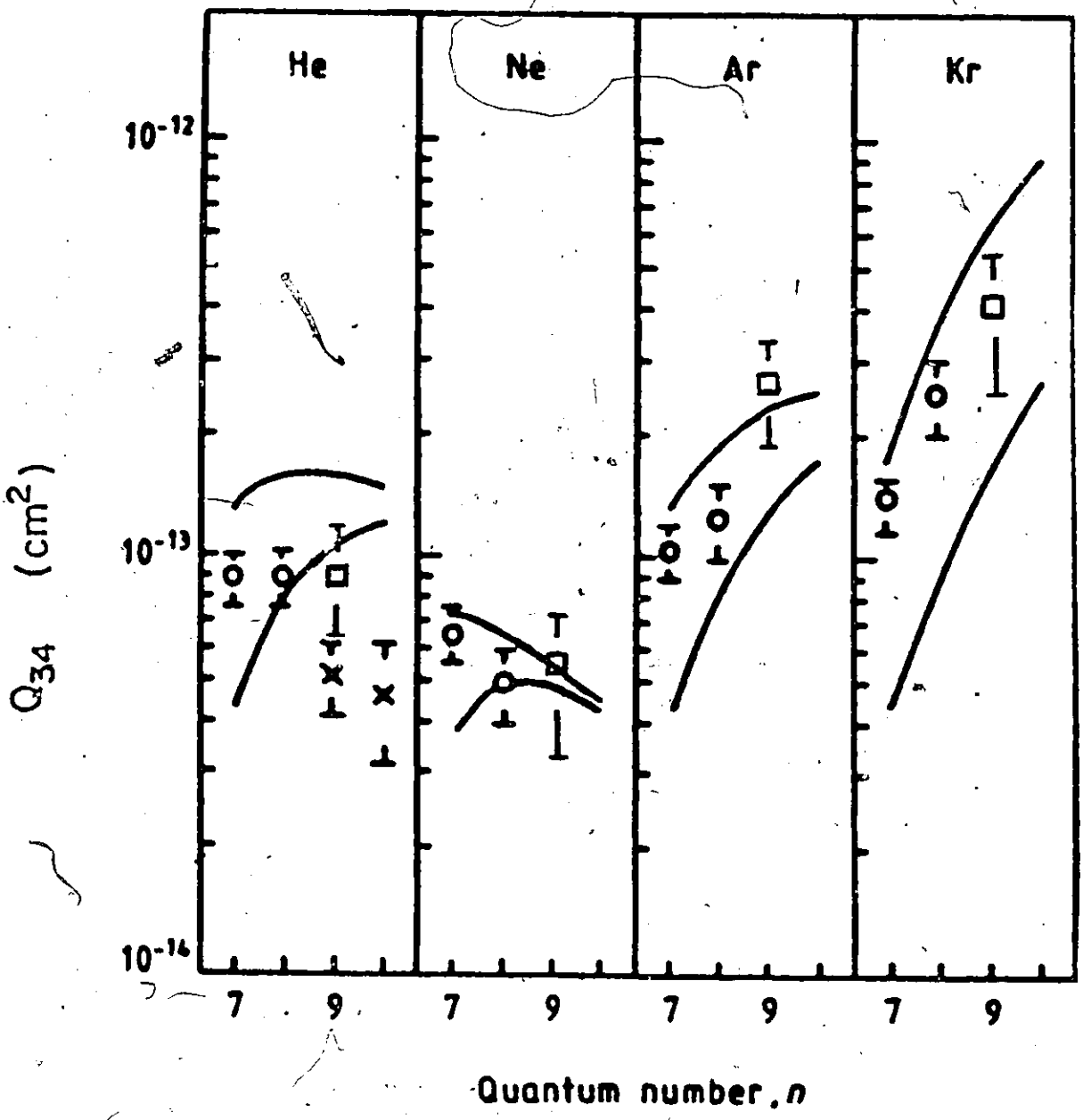

Table 4: $9^2D_{3/2} \leftrightarrow 9^2D_{5/2}$ Fine-structure Mixing Cross Sections
($10^{-14}cm^2$)

Collision Partners	Q_{34} $(9^2D_{3/2} \rightarrow 9^2D_{5/2})$	Q_{43} $(9^2D_{3/2} \leftarrow 9^2D_{5/2})$	$\frac{Q_{34}}{Q_{43}}$	Ref.
Rb-He	9±3 5.1±1	6±2	1.45	This work 6
Rb-Ne	6±2	3±1	1.91	This work
Rb-Ar	26±9	17±6	1.50	This work
Rb-Kr	42±15	23±8	1.79	This work

Table 5: $n^2D_{3/2} \leftrightarrow n^2D_{5/2}$ Fine-structure Mixing Cross Sections for Collisions with He
$(10^{-14}cm^2)$

State	Q_{34}	Q_{43}	$\frac{Q_{34}}{Q_{43}}$	Q_3	Q_4	Ref.
6 D	6.6±1.0	4.5±0.7	1.47	0±4	0.4±3	8
7 D	8.8±1.3	5.8±0.9	1.51	1.1±0.3	0.3±0.1	8
8 D	8.9±1.4	5.8±0.9	1.51	0.3±0.3	0.4±0.3	8
9 D	9±3	6±2	1.45	8±9	0.0±0.6	this work

Table 6: $n^2D_{3/2} \leftrightarrow n^2D_{5/2}$ Fine-structure Mixing Cross Sections for Collisions with Ne
$(10^{-14}cm^2)$

State	Q_{34}	Q_{43}	$\frac{Q_{34}}{Q_{43}}$	Q_3	Q_4	Ref.
6 D	6.1±0.9	4.1±0.6	1.48	0.7±0.7	0.0±0.5	8
7 D	6.5±1.0	4.0±0.6	1.62	0.2±0.1	0.2±0.1	8
8 D	4.9±1.0	3.2±0.6	1.53	0.2±0.2	0.2±0.2	8
9 D	6±2	3±1	1.91	.12±.15	0.8±1	This work

Table 7: $n^2D_{3/2} \leftrightarrow n^2D_{5/2}$ Fine-structure Mixing Cross Sections for Collisions with Ar
$(10^{-14}cm^2)$

State	Q_{34}	Q_{43}	$\frac{Q_{34}}{Q_{43}}$	Q_3	Q_4	Ref.
6 D	5.3±0.8	3.6±0.6	1.48	0.5±0.6	0.0±0.2	8
7 D	10.4±1.6	6.9±1.0	1.50	0.1±0.1	0.5±0.5	8
8 D	12.4±2.3	9.4±1.9	1.32	0.7±0.7	0.5±0.5	8
9 D	26±9	17±6	1.50	0.4±0.5	0±0.05	This work

Table 8: $n^2D_{3/2} \leftrightarrow n^2D_{5/2}$ Fine-structure Mixing Cross Sections for Collisions with Kr
$(10^{-14}cm^2)$

State	Q_{34}	Q_{43}	$\frac{Q_{34}}{Q_{43}}$	Q_3	Q_4	Ref.
6 D	8.5±1.3	5.5±0.8	1.55	0.2±0.3	0.5±0.4	8
7 D	14.1±1.5	9.0±1.0	1.57	0.3±0.2	0.2±0.2	8
8 D	24.9±5	15.1±3.0	1.65	0.7±0.8	0.8±1.0	8
9 D	42±15	26±8	1.79	0±6	7±4	This work

V. CONCLUSION AND SUMMARY

The two-photon absorption technique was used to selectively excite the 9 ^{2}D fine-structure sub-states of Rb atoms in pure Rb vapour or in a mixture with He, Ne, Ar, or Kr. The resulting fluorescence was separated into its spectral components, registered with a photon counter and the cross sections for $9^2D_{3/2} \leftrightarrow 9^2D_{5/2}$ fine-structure mixing and quenching were determined from the measured ratios of the fluorescence intensities. The results are listed in Tables 3 and 4.

From this data it is possible to make the following conclusion:

a) The cross sections for collisions with noble gases range from 3×10^{-14} cm^2 to 42×10^{-14} cm^2.

b) The variation of the cross sections with the principal quantum number n is in good agreement with the predictions of the theory proposed by Sirko and Rosinski.[16]

c) The variation of the cross sections Q_{43} with the atomic number of the noble-gas perturber follows a trend similar to that followed by the free electron-noble gas total scattering cross sections although the Q_{43} values are larger than the total electron scattering cross

sections.

d) As expected, the cross section for Rb*-Rb collisions was more than an order of magnitude larger than the Rb-noble gas cross sections, because of the long range of the interaction. The Rb*-Rb cross section was found to be of comparable magnitude to the geometrical cross section.

BIBLIOGRAPHY

1 R.W. Wood and L. Dunoyer, Phil. Mag., 27, 1018 (1914); R.W. Wood and F.L. Mohler, Phys. Rev., 11, 70 (1918).

2 B. Pitre, A.Rae and L. Krause, Can. J. Phys., 44, 731 (1966).

3 T.J. Beahn, W.J. Condell and H.I. Mandelberg, Phys. Rev., 141, (1966).

4 A. Gallagher, Phys. Rev., 157, 68 (1967).

5 F. Gounand, P. R. Fournier, and J. Berlande, Phys. Rev. A, 15, 2212 (1977).

6 M. Hugon, F. Gounand, and P,R. Fournier, J. Berlande, J. Phys.B, 13, 1585 (1980).

7 J. Wolnikowski, J.B. Atkinson, J. Supronowicz and L. Krause, Phys. Rev. A, 25, 2622 (1982).

8 J.S. Supronowicz, PhD. Thesis, University of Windsor (1985).

9 R.H. Hill, H.A. Schuessler and B.G. Zollars, Phys. Rev. A, 24, (1981).

10 T.F. Gallagher, R.A. Safinya and G.A. Ruff, Phys. Rev. A, 27, 2222 (1983).

11 L. Sirko and K. Rosinski, J. Phys. B, 18, L221 (1985).

12 R.W. Berends, W. Kedzierski and L.Krause, J. Quant. Spectrosp. Radiat. Transfer, 37, 157 (1987).

13 E. de Prunelé and J. Pascale, J. Phys. B, 12, 2511 (1979).

14 A. Omont, J Physique, 38, 1343 (1977).

15 Y. Hahn, J. Phys. B, 14, 985 (1981).

16 L.Sirko and K. Rosinski, J. Phys. B, 19, L279 (1986).

17 The separation of the Rb nD level from the (n+2)S level is more than a hundred times larger than the fine-structure splitting:
($9\,D \leftrightarrow 11S$)=95cm^{-1}; ($9\,D_{2/3} \leftrightarrow 9D_{5/2}$)=0.70cm^{-1}

18 H.S.W. Massey, Electronic and Ionic Impact Phenomena, Vol.III, (Oxford University Press, London, 1971).

19 A.P. Hickman, J.Phys. B, 14,L419 (1981).

20 H.A. Bethe and E.E. Salpeter, Quantum Mechanics of One-and Two-Electron Atoms, (Plenum Publishing Corporation, New York, 1977).

21 P. Pace and J.B. Atkinson, Can. J. Phys., 52, 1635 (1974).

22 G. Woodgate, Elementary Atomic Structure, (McGraw-Hill, London, 1971).

23 J. Migdalek and W.E. Baylis, Can. J. Phys., 57, 1708 (1979).

24 G. Waligorski, P. Kowalczyk and C. Radzewicz, J. Phys. D, 3, 79 (1986).

25 F. Gounand, M. Hugon and P.R. Fournier, J. Physique, 41, 119 (1980).

26 J. Marek and P. Munster, J. Phys. B, 13, 1731 (1980).

27 A. Lindgärd, S.E. Nielsen, Atomic Data Nucl. Data Tables, 19, 533 (1977).

28 P. Grudzev, and V.I. Denisov, Opt and Spect., 52, 8 (1982).

29 C.E. Theodosiou, Phys. Rev. A 30, 2881 (1984).

30 M.G. Littman, Optics Letters, 3, 138 (1978).

31 A. Nesmeyanov, Vapour Pressures of the Elements, (Academic Press, New York, 1963).

32 M. Hugon, F. Gounand and P.R. Fournier, J. Phys. B, 13, L109 (1980)

33 F. Gounand, P.R. Fournier, M. Hugon, XI International Conference on the Physics of Electronic and Atomic Collisions, Edited by K. Takayanaki, and N. Oda, (The Society for Atomic Collision Research, Kyoto, 1979).

34 J.W. Parker, H.A. Schuessler, R.H. Hill and B.G. Zollars, Phys. Rev. A 29, 617 (1984).

35 J. Supronowicz, J.B. Atkinson and L. Krause, Phys. Rev. A, 30, 112 (1984).

36 B.G. Zollars, H.A. Schuessler, J.W. Parker and R.H. Hill Jr., Phys. Rev. A, 28,1329 (1983).

37 M. Hugon, B. Sayer, P.R. Fournier,and F. Gounand, J.Phys. B, 15, 2391 (1982).

38 A. Stone, Radiation and Optics, (McGraw-Hill Book Company Inc., New York, 1963).

VITA AUCTORIS

I was born on February 20, 1962 in Pullman Washington. In 1969 I moved to Winnipeg, Manitoba where I attended elementary and secondary school. Upon graduation in 1980 I enrolled in a combined program of mathematics and physics at the University of Winnipeg. After receiving my degree in 1986, I enrolled in the Faculty of Graduate Studies at the University of Windsor to work towards a Masters degree in Physics.